Tokyo Climate Center, Japan Meteorological Agency

TCC News

Autumn 2020

Table of Contents: TCC News No. 62

El Niño Outlook (December 2020 – June 2021)

La Niña conditions are considered to have persisted in the equatorial Pacific since boreal summer. La Niña conditions are likely (90%) to continue through boreal winter, and are also considered more likely to continue until boreal spring (60%) than a return of ENSO neutral conditions (40%) (article based on the El Niño outlook issued on 10 December 2020).

1. El Niño/La Niña

- In November 2020, the NINO.3 SST was below normal with a deviation of-1.2°C. SSTs in the equatorial Pacific were above normal in the western part and below normal in central and eastern parts (Figures 1-1 and 1-3 (a)), while subsurface temperatures were above normal in the western part and below normal in central and eastern parts (Figures 1-2 and 1-3 (b)). Atmospheric convective activity near the date line over the equatorial Pacific was below normal, and easterly winds in the lower troposphere (i.e., trade winds) over the central equatorial Pacific were stronger than normal. These oceanic and atmospheric conditions were also commonly seen in past La Niña events. La Niña conditions are considered to have persisted in the equatorial Pacific since boreal summer.
- The subsurface cold waters, observed in the central and eastern equatorial Pacific in November, are expected to maintain colder-than-normal SST conditions in the eastern part through boreal winter. JMA's El Niño prediction model suggests that the NINO.3 SST will be below normal through boreal winter before gradually approaching the normal (Figure 1-4). La Niña conditions are likely (90%) to continue through boreal winter, and are also considered more likely to continue until boreal spring (60%) than a return of ENSO neutral conditions (40%) (Figure 1-5).

2. Western Pacific and Indian Ocean

The area-averaged SST in the tropical western Pacific (NINO.WEST) region was above normal in November, and values are likely to be above or near normal until boreal spring. The area-averaged SST in the tropical Indian Ocean (IOBW) region was near normal in November, and values are likely to be near or below normal until boreal spring.

(UMEDA Takafumi, Tokyo Climate Center)

* The SST normal for the NINO.3 region (5°S – 5°N, 150°W – 90°W) is defined as an monthly average over the latest sliding 30-year period (1990-2019 for this year).

* The SST normals for the NINO.WEST region (Eq. – 15°N, 130°E – 150°E) and the IOBW region (20°S – 20°N, 40°E – 100°E) are defined as linear extrapolations with respect to the latest sliding 30-year period, in order to remove the effects of significant long-term warming trends observed in these regions.

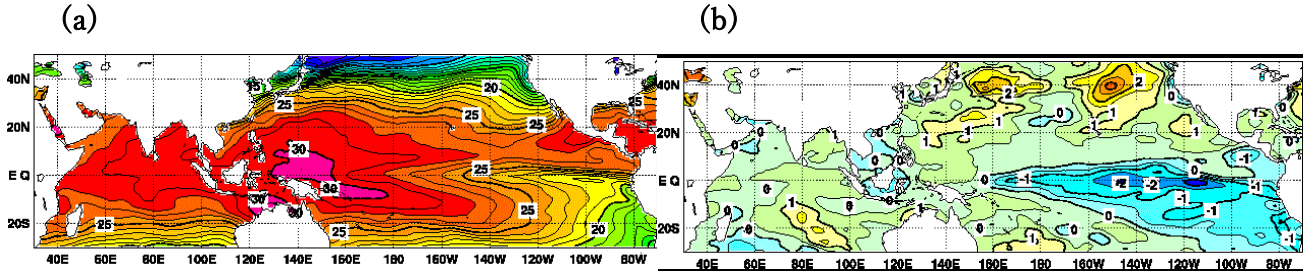

Figure 1-1 Monthly mean (a) sea surface temperatures (SSTs) and (b) SST anomalies in the Indian and Pacific Ocean areas for October 2020

The contour intervals are 1℃ in (a) and 0.5℃ in (b). The base period for the normal is 1981 – 2010.

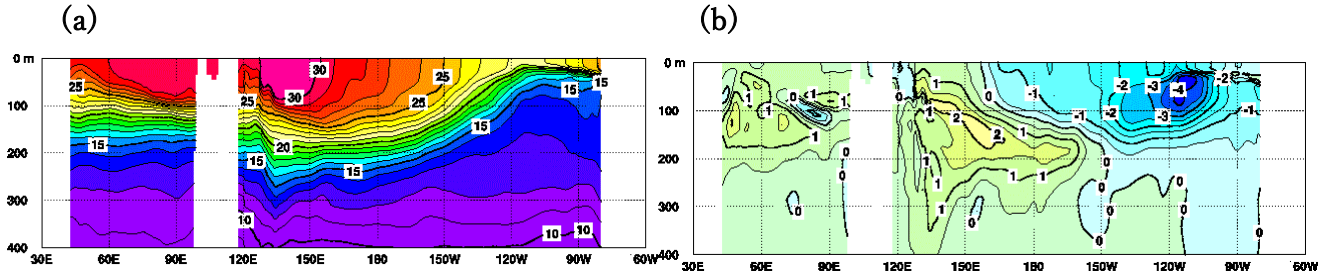

Figure 1-2 Monthly mean depth-longitude cross sections of (a) temperature and (b) temperature anomalies in the equatorial Indian and Pacific Ocean areas for November 2020

Contour intervals are 1℃ in (a) and 0.5℃ in (b). The base period for the normal is 1981 – 2010.

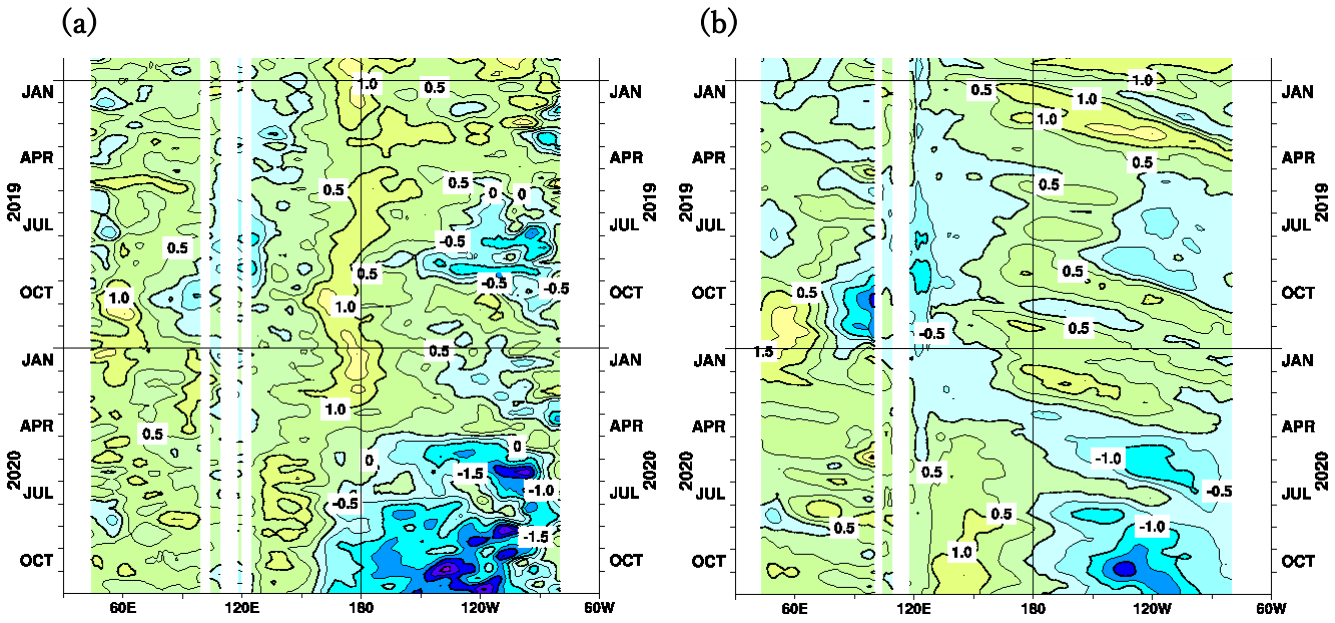

Figure 1-3 Time-longitude cross sections of (a) SST and (b) ocean heat content (OHC) anomalies along the equator in the Indian and Pacific Ocean areas

OHCs are defined here as vertically averaged temperatures in the top 300 m. The base period for the normal is 1981 – 2010.

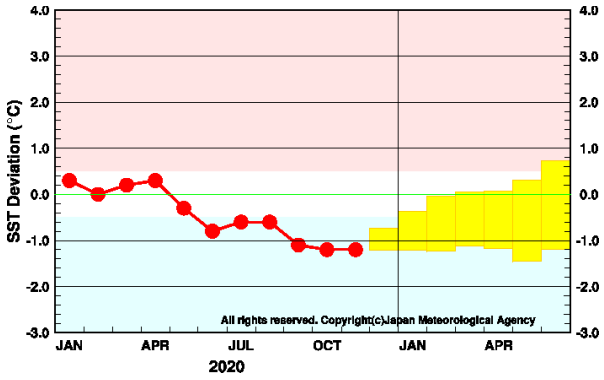

Figure 1-4 Outlook of NINO.3 SST deviation produced by the El Niño prediction model

This figure shows a time series of monthly NINO.3 SST deviations. The thick line with closed circles shows observed SST deviations, and the boxes show the values produced for up to six months ahead by the El Niño prediction model. Each box denotes the range into which the SST deviation is expected to fall with a probability of 70%.

YEAR	MONTH	mean period	El Niño	ENSO neutral	La Niña
2020	OCT	AUG2020–DEC2020	10	90	
	NOV	SEP2020–JAN2021	10	90	
	DEC	**OCT2020–FEB2021**	10	90	
2021	**JAN**	**NOV2020–MAR2021**	10	90	
	FEB	**DEC2020–APR2021**	20	80	
	MAR	**JAN2021–MAY2021**	40	60	
	APR	**FEB2021–JUN2021**	50	50	

Figure 1-5 ENSO forecast probabilities based on the El Niño prediction model

Red, yellow and blue bars indicate probabilities that the five-month running mean of the NINO.3 SST deviation from the latest sliding 30-year mean will be +0.5°C or above (El Niño), between +0.4 and -0.4°C (ENSO-neutral) and -0.5°C or below (La Niña), respectively. Regular text indicates past months, and bold text indicates current and future months.

<<Table of contents <Top of this article

JMA's Seasonal Numerical Ensemble Prediction for Boreal Winter 2020/2021

This report outlines JMA's dynamical seasonal ensemble prediction for boreal winter 2020/2021 (December – February, referred to as DJF), which was used as a basis for JMA's operational cold-season outlook issued on 25 November 2020. The outlook is based on the seasonal ensemble prediction system of the Coupled Atmosphere-ocean General Circulation Model (CGCM).

Summary: Based on JMA's seasonal ensemble prediction system, sea surface temperature (SST) anomalies are expected to be below normal in the central-to-eastern equatorial Pacific during boreal winter 2020/2021, suggesting a continuation of La Niña conditions. In association with above-normal SSTs in and around the Maritime Continent, active convection is expected from the eastern tropical Indian Ocean to Southeast Asia, resulting in positive anomalies of the stream function at 200 hPa and a northward shift of the subtropical jet over southern Eurasia.

1. SST anomalies (Figure 2-1)

Figure 2-1 shows predicted SSTs (contours) and related anomalies (shading) for DJF. Below-normal anomalies are expected in the central-to-eastern equatorial Pacific. As subsurface ocean temperature anomalies in the eastern part of the equatorial Pacific are expected to be below normal (not shown), La Niña conditions are likely to continue during the period. Near-normal SST anomalies are expected over the equatorial Indian Ocean, suggesting that IOD-like conditions are not necessarily expected.

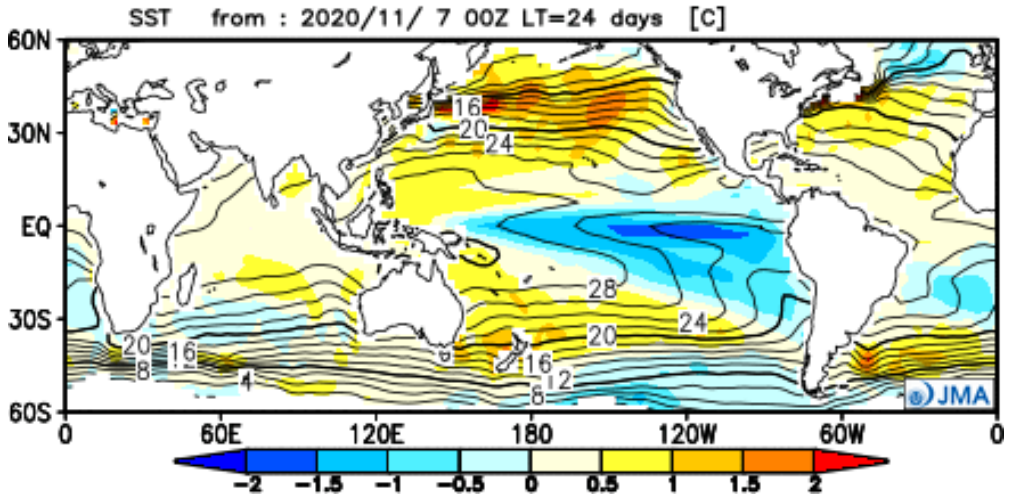

Figure 2-1 Predicted SSTs (contours) and SST anomalies (shading) for December–February 2020/2021 (ensemble mean of 51 members)

2. Prediction for the tropics and sub-tropics (Figure 2-2)

Figure 2-2 (a) shows predicted precipitation (contours) and related anomalies (shading) for DJF. In association with above-normal SSTs in and around the Maritime Continent, above-normal anomalies are expected over Southeast Asia. Below-normal anomalies are expected around the date line in the equatorial Pacific.

Figure 2-2 (b) shows predicted velocity potential (contours) and related anomalies (shading) at the upper troposphere (200 hPa) for DJF. In association with the predicted SST and precipitation anomalies detailed above, negative (i.e., divergent) anomalies are expected from the eastern tropical Indian Ocean to Southeast Asia, while

positive (i.e., convergent) anomalies are expected over the western-to-central tropical Pacific.

Figure 2-2 (c) shows predicted stream functions (contours) and related anomalies (shading) at the upper troposphere (200 hPa) for DJF. Equatorial symmetric cyclonic (i.e., negative in the Northern Hemisphere) anomalies are expected over the central tropical Pacific. Anti-cyclonic (i.e., positive) anomalies are expected over southern Eurasia, indicating a northward shift of the subtropical jet stream's axis over the region.

Figure 2-2 (d) shows predicted stream functions (contours) and related anomalies (shading) at the lower troposphere (850 hPa) for DJF. In association with active convection over the eastern tropical Indian Ocean, equatorial symmetric cyclonic (i.e., negative in the Northern Hemisphere) anomalies are predicted over the Indian Ocean. Equatorial symmetric anti-cyclonic (i.e., positive in the Northern Hemisphere) anomalies are expected over the Pacific Ocean in association with inactive convection over the western-to-central tropical Pacific.

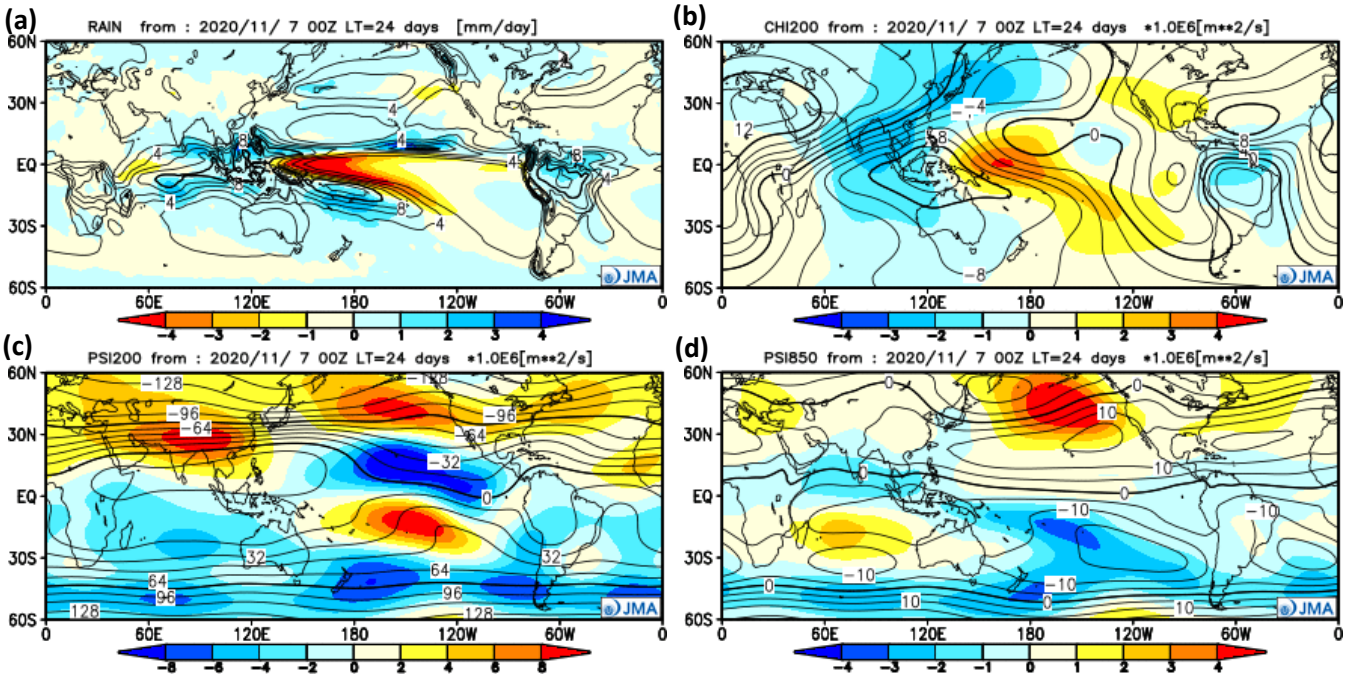

Figure 2-2 Predicted atmospheric fields from 60°N-60°S for December-February 2020/2021 (ensemble mean of 51 members)
(a) Precipitation (contours) and anomaly (shading). The contour interval is 2 mm/day. (b) Velocity potential at 200 hPa (contours) and anomaly (shading). The contour interval is 2×10^6 m^2/s. (c) Stream function at 200 hPa (contours) and anomaly (shading). The contour interval is 16×10^6 m^2/s. (d) Stream function at 850 hPa (contours) and anomaly (shading). The contour interval is 5×10^6 m^2/s.

3. Prediction for the mid- and high- latitudes of the Northern Hemisphere (Figure2-3)

Figure 2-3 (a) shows predicted geopotential heights (contours) and related anomalies (shading) at 500 hPa for DJF. Positive anomalies are predicted for most of the Northern Hemisphere except over Japan and in and around Alaska.

Figure 2-3 (b) shows predicted sea level pressure (contours) and related anomalies (shading) for DJF. In association with relatively large anomalies in the geopotential height at 500 hPa, positive anomalies are expected over the northern part of the North Pacific and the North Atlantic. Negative anomalies are predicted over the Laptev Sea and Japan.

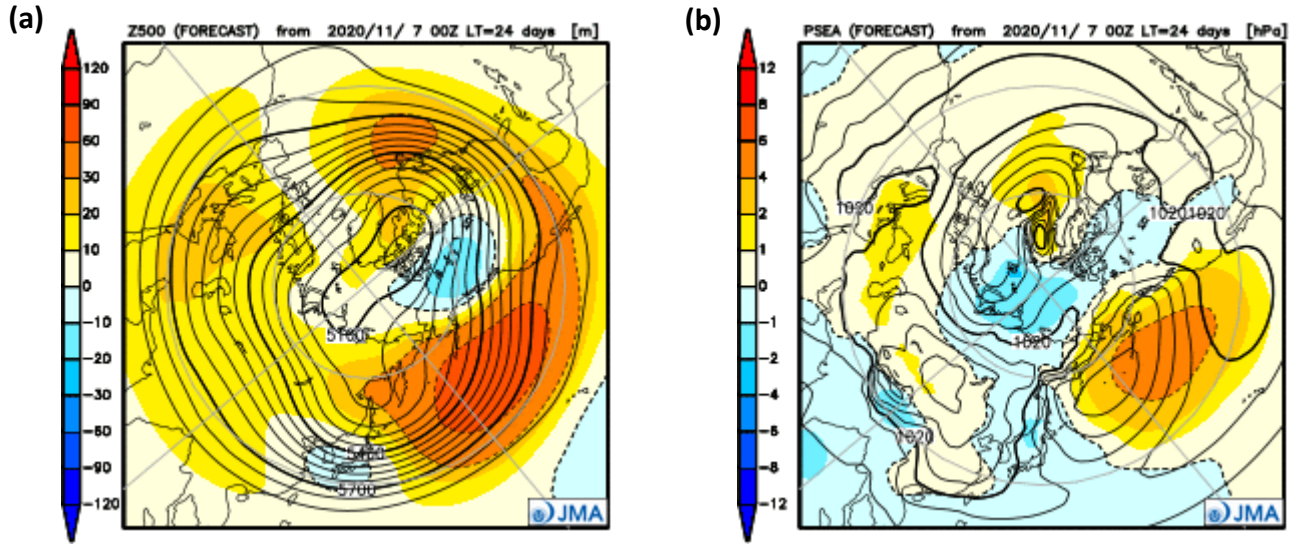

Figure 2-3 Predicted atmospheric fields from 20°N-90°N for December-February 2020/2021 (ensemble mean of 51 members)
(a) Geopotential height at 500 hPa (contours) and anomaly (shading). The contour interval is 60 m. (b) Sea level pressure (contours) and anomaly (shading). The contour interval is 4 hPa.

Note: JMA operates a seasonal Ensemble Prediction System (EPS) using the Coupled atmosphere-ocean General Circulation Model (CGCM) to make seasonal predictions beyond a one-month time range. The EPS produces perturbed initial conditions by means of a combination of the initial perturbation method and the lagged average forecasting (LAF) method. The prediction is made using 51 members from the latest four initial dates (13 members are run every 5 days). Details of the prediction system and verification maps based on 30-year hindcast experiments (1981–2010) are available at https://ds.data.jma.go.jp/tcc/tcc/products/model/.

(ISHIZAKI Shiro, Tokyo Climate Center)

<<Table of contents <Top of this article

Summary of the 2020 Asian Summer Monsoon

1. Precipitation and temperature

CLIMAT data on four-month total precipitation for the summer monsoon season (June – September) show more than 140% of the normal in the eastern part of East Asia, the southeastern part of Southeast Asia and southern/western parts of South Asia, while values less than 60% of the normal were seen in the northeastern part of Southeast Asia and western China (Figure 3-1 (a)). Seasonal precipitation in China from June to August was the second highest since 1961 (China Meteorological Administration), and monthly precipitation in western/eastern Japan for July was the highest since 1946. Heavy rain caused more than 270 fatalities or people missing in China from June to August (Chinese Government), 84 fatalities in Japan in July (Fire and Disaster Management Agency of Japan) and more than 2,200 fatalities in/around South Asia from June to September (governments of India/Nepal/Pakistan, European Commission).

Four-month mean temperatures for the same period were above normal in many parts of Asia, while values were below normal in and around the northwestern part of East Asia (Figure 3-1 (b)). Monthly mean temperatures in western and eastern Japan for August were the highest since 1946. Heat waves caused a total of 112 fatalities in Japan from June to September (Fire and Disaster Management Agency of Japan).

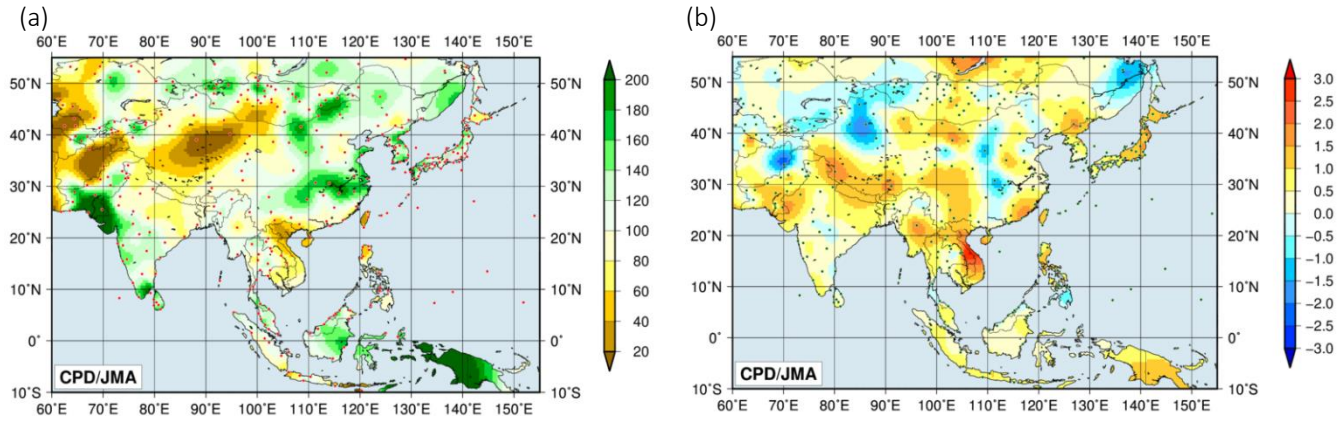

Figure 3-1 Four-month (a) precipitation ratios [%] and (b) mean temperature anomalies [°C] from June to September 2020
The base period for the normal is 1981 – 2010. The red (a) and green (b) dots show stations providing map data, which are interpolated due to a lack of CLIMAT reporting and climatological normal values in some areas.

2. Tropical cyclones

A total of 13 named tropical cyclones (TCs) had formed over the western North Pacific and the South China Sea by September 2020, as compared to the normal of 18.4 (Table 3-1). From June to September, 12 named TCs (climatological normal: 16.0) formed, with 10 approaching or making landfall on East Asia and 6 (climatological normal: 9.2) approaching Japan. No named TCs formed in July for the first time since 1951.

Between late August and early September, 3 TCs (Bavi, Maysak and Haishen) reaching TY intensity passed by Okinawa/Amami and made landfall on the Korean Peninsula.

Table 3-1 Tropical cyclones reaching TS intensity or higher formed over the western North Pacific and the South China Sea by September 2020

Name (number)		Date (UTC)	Category[1)]	Maximum wind[2)] (kt)
Vongfong	(2001)	12 May - 16 May	TY	85
Nuri	(2002)	12 Jun - 13 Jun	TS	40
Sinlaku	(2003)	1 Aug - 2 Aug	TS	40
Hagupit [3)]	(2004)	1 Aug - 5 Aug	TY	70
Jangmi [3)]	(2005)	8 Aug - 10 Aug	TS	45
Mekkhala [3)]	(2006)	10 Aug - 11 Aug	STS	50
Higos [3)]	(2007)	18 Aug - 19 Aug	STS	55
Bavi [3)]	(2008)	22 Aug - 27 Aug	TY	85
Maysak [3)]	(2009)	28 Aug - 3 Sep	TY	95
Haishen [3)]	(2010)	1 Sep - 7 Sep	TY	100
Noul [3)]	(2011)	15 Sep - 18 Sep	TS	45
Dolphin [3)]	(2012)	21 Sep - 24 Sep	STS	60
Kujira [3)]	(2013)	27 Sep - 30 Sep	STS	60

Note: Based on information from the RSMC Tokyo-Typhoon Center.
1) Intensity classification for tropical cyclones.
TS: tropical storm, STS: severe tropical storm, TY: typhoon
2) Estimated maximum 10-minute mean wind.
3) Based on early analysis data, but not best track.

3. Monsoon activity and atmospheric circulation

Convective activity inferred from OLR averaged for June – September 2020 (Figure 3-2) was enhanced over the western tropical Indian Ocean and the Maritime Continent, and was suppressed from the northern part of Southeast Asia to the central equatorial Pacific in association with higher-than-normal SSTs in the tropical Indian Ocean and La Niña conditions in the equatorial Pacific (Figure 3-3). OLR index data (Table 3-2) indicate that the overall activity of the Asian summer monsoon (represented by the SAMOI (A) index) was below normal, and the active convection area was shifted southward (SAMOI (N) index) and westward (SAMOI (W) index) of its normal position except in August.

In the upper troposphere (Figure 3-4 (a)), cyclonic circulation anomalies straddling the equator were seen over the Maritime Continent, while anti-cyclonic circulation anomalies straddling the equator were seen from Africa to the central Indian Ocean with the westward extension of the Tibetan High. The southward displacement of the subtropical jet stream (STJ) over Eurasia was related to weaker-than-normal northward extension of the Tibetan High, which is likely attributable to the suppressed convective activity observed over the monsoon region. A wave train along the STJ was seen, with cyclonic circulation anomalies over Central Asia and anti-cyclonic circulation anomalies over southern China and to the east of Japan.

In the lower troposphere (Figure 3-4 (b)), cyclonic circulation anomalies straddling the equator were seen over the western tropical Indian Ocean, while anti-cyclonic circulation anomalies straddling the equator were seen from the eastern tropical Indian Ocean to the western tropical Pacific. The North Pacific Subtropical High (NPSH) extended southwestward of its climatological extent, and the monsoon trough over Southeast Asia was weaker than normal. Figure 3-5 shows northeasterly surface wind anomalies extending from the northeastern Indian Ocean to the western

tropical North Pacific, which imply low-level divergence anomalies over areas from the South China Sea to the western tropical North Pacific. The lower-tropospheric divergence anomalies gave rise to descending air flow and suppressed convective activity over these areas, which likely contributed to the southwestward extension of the NPSH.

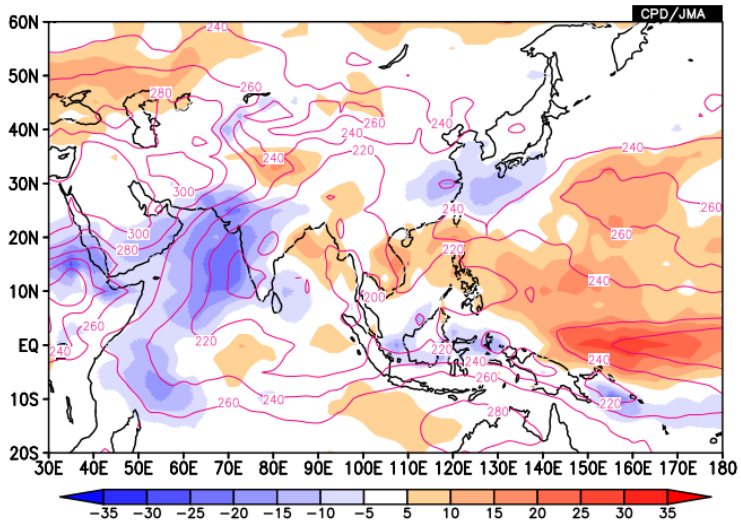

Figure 3-2 Four-month mean outgoing longwave radiation (OLR) [W/m^2] for June–September 2020
The contours indicate OLR at intervals of 20 W/m^2, and the color shading denotes OLR anomalies from the normal (i.e., the 1981–2010 average). Negative (cold color) and positive (warm color) OLR anomalies show enhanced and suppressed convection compared to the normal, respectively. Original data are provided by NOAA.

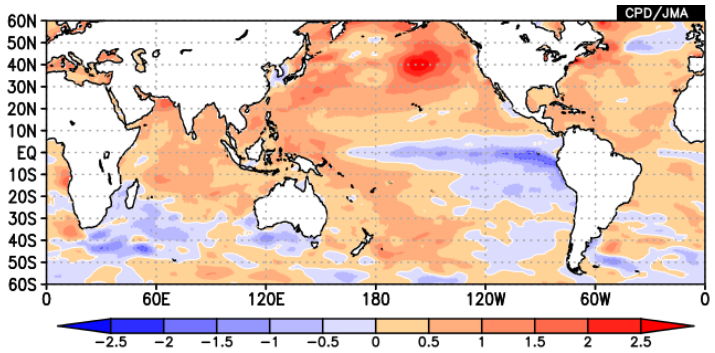

Figure 3-3 Four-month mean sea surface temperature (SST) anomalies [°C] for June–September 2020
The base period for the normal is 1981 – 2010.

Table 3-2 Summer Asian Monsoon OLR Index (SAMOI) values observed from May to September 2020
Asian summer monsoon OLR indices (SAMOI) are derived from OLR anomalies. SAMOI (A), (N) and (W) indicate the overall activity of the Asian summer monsoon, its northward shift and its westward shift, respectively. SAMOI definitions are as follows: SAMOI (A) = (-1) × (W + E); SAMOI (N) = S – N; SAMOI (W) = E – W. W, E, N and S indicate area-averaged OLR anomalies for the respective regions shown in the figure on the right normalized by their standard deviations.

	Summer Asian Monsoon OLR Index (SAMOI)		
	SAMOI (A): Activity	SAMOI (N): Northward-shift	SAMOI (W): Westward-shift
May 2020	-1.0	-1.4	+0.8
Jun 2020	-0.7	-1.0	+0.3
Jul 2020	-1.7	-0.8	+0.2
Aug 2020	-0.9	+1.7	-0.2
Sep 2020	-0.1	-0.3	+1.9

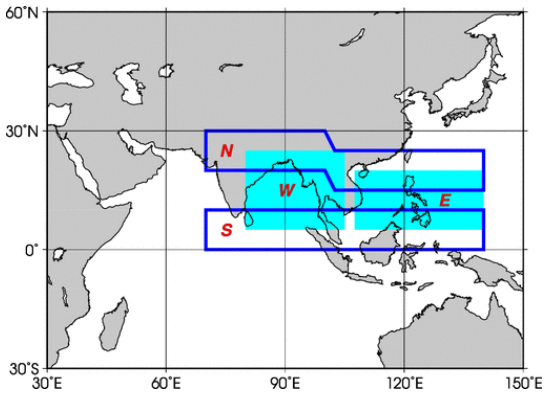

(a) (b)

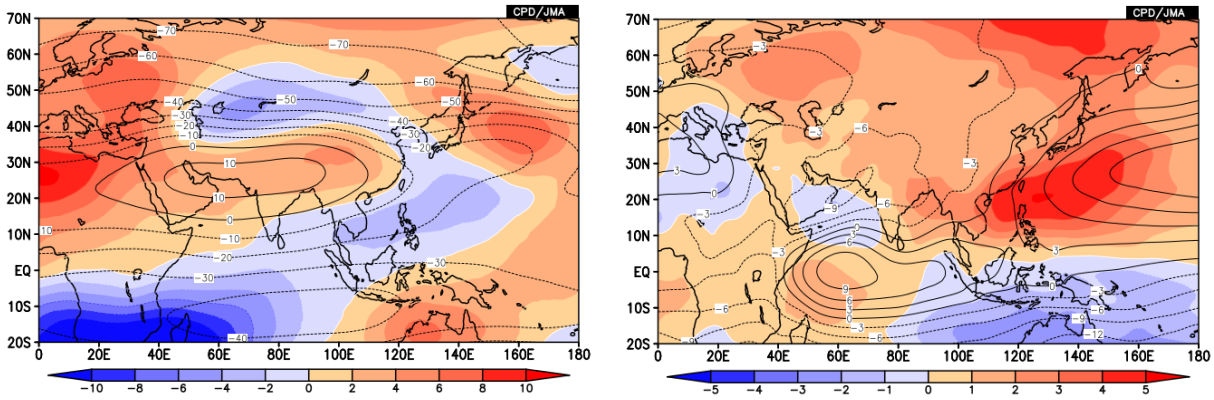

Figure 3-4 Four-month mean (a) 200-hPa and (b) 850-hPa stream function [10^6 m^2/s] for June–September 2020
Contours indicate stream function at intervals of (a) 10 × 10^6 m^2/s and (b) 3 × 10^6 m^2/s, and shading shows stream function anomalies. Red (blue) shading denotes anti-cyclonic (cyclonic) circulation anomalies in the Northern Hemisphere, and vice-versa in the Southern Hemisphere. The base period for the normal is 1981 – 2010.

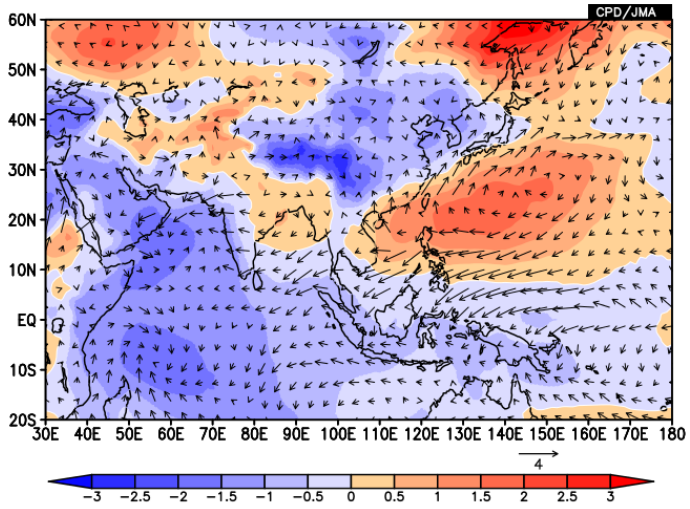

Figure 3-5 Sea level pressure anomalies (color shading) [hPa] and surface wind vector anomalies (vectors) [m/s] for June–September 2020.
The base period for the normal is 1981 – 2010.

In July 2020, areas from western to northeastern Japan experienced record-heavy rain and record-low sunshine durations. These phenomena are attributed to a continued tendency for large amounts of water vapor to concentrate around western and eastern Japan from two major flows (Figure 3-6) – one from the west along the active Meiyu-Baiu front, which stagnated from central China to mainland Japan due to delayed northward migration of the STJ, and the other from the southwest along the periphery of the NPSH, which extended southwestward of its climatological extent (Figure 3-7). A persistent upper-level trough over the Yellow Sea, which was sustained by quasi-stationary Rossby wave propagation along the STJ over Eurasia (Figure 3-7 (a)), also caused an intensification of Meiyu-Baiu front activity with enhanced vertical upward flow over western and eastern Japan, resulting in prolonged heavy rain.

In August 2020, the STJ migrated northward over East Asia due to the northward shift of active convection over the Asian monsoon region, and also meandered northward over Japan due to Rossby wave propagation along the STJ with a geographical phase different from that observed in July. In association with this meandering, the NPSH and the Tibetan High expanded toward Japan and brought record-high temperatures in western and eastern parts of the country via strengthened downward flow and predominant sunny conditions.

(a) (b)

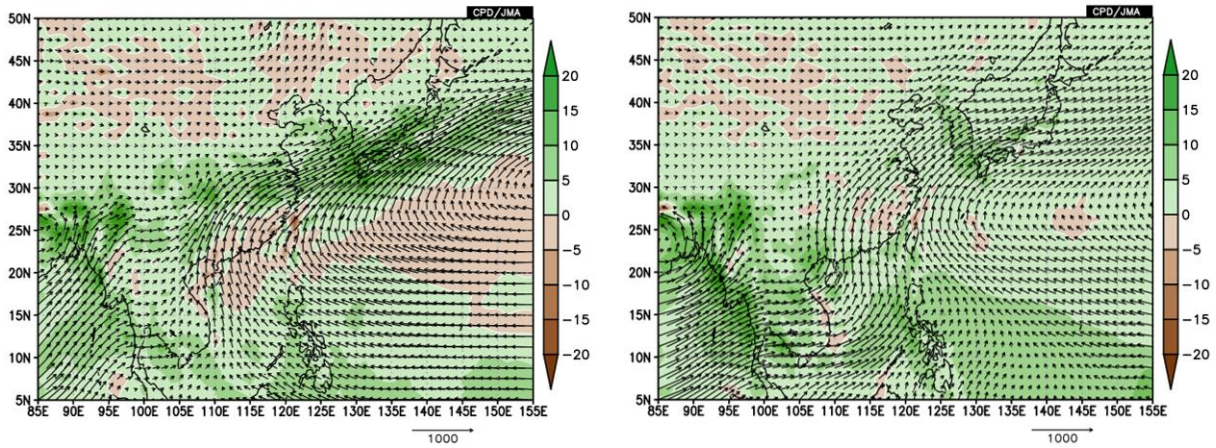

Figure 3-6 Monthly mean vertically integrated horizontal water vapor flux (arrows) and related convergence (color shading): (a) July 2020; (b) normal

Unit: kg/m/s for arrows and mm/day for shading. Green (brown) shading denotes convergence (divergence). Vertical integration is up to 300 hPa. The base period for the normal is 1981 – 2010.

(a) (b)

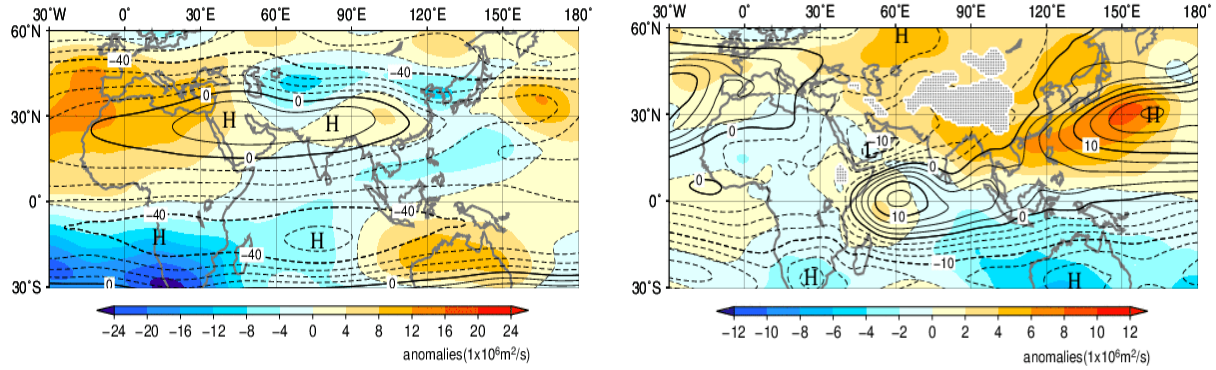

Figure 3-7 Monthly mean (a) 200-hPa and (b) 850-hPa stream function [10^6 m^2/s] for July 2020

Contours indicate stream function at intervals of (a) 10×10^6 m^2/s and (b) 2.5×10^6 m^2/s, and shading shows stream function anomalies. Hatch patterns indicate areas with altitudes exceeding 1,600 m. The base period for the normal is 1981 – 2010.

(SATO Hitoshi, Tokyo Climate Center)

<<Table of contents <Top of this article

Status of the Antarctic Ozone Hole in 2020

The size of the Antarctic ozone hole in 2020 exceeded the most recent decadal average due to a large low-temperature area in the stratosphere. In the long term, however, a statistically significant decreasing trend in the maximum size has been observed since 2000.

Since the early 1980s, the Antarctic ozone hole has appeared every year in austral spring with a peak in September or early October. It is generally defined as the area in which the total ozone column value is below 220 m atm-cm.

JMA analysis based on data from the Ozone Mapper Profiler Suite (OMPS) aboard the Suomi National Polar-orbiting Partnership (NPP) satellite indicates that the 2020 Antarctic ozone hole appeared in mid-August and expanded rapidly from late August onward, exceeding the scale of the most recent decadal average (Figure 4-1, upper left). Its maximum size for the year (observed on 20 September) was 24.6 million square kilometers (Figure 4-1, upper right), which is 1.8 times as large as the Antarctic itself. In 2020 the polar vortex over Antarctica was stable and dominant, and the low-temperature area in the stratosphere was larger than the most recent decadal average after mid-July. These conditions contributed to the year's expanded ozone hole via increased formation of polar stratospheric clouds (PSCs), which play an important role in ozone depletion.

As an overall trend, the maximum size of the Antarctic ozone hole has shown a statistically significant decrease since 2000. The WMO/UNEP Scientific Assessment of Ozone Depletion: 2018 report detailed how the hole is expected to close gradually, with springtime total column ozone in the 2060s returning to 1980 values.

The ozone layer acts as a shield against ultraviolet radiation, which can cause skin cancer. The ozone hole was first recognized in the early 1980s, and large-scale events have been observed since the 1990s. Its record size was 29.6 million square kilometers (2000). The Antarctic ozone hole significantly affects summer climatic conditions on the surface of the Southern Hemisphere according to the recent assessment.

(KIMURA Mika, Atmospheric Environment and Ocean Division)

<<Table of contents <Top of this article

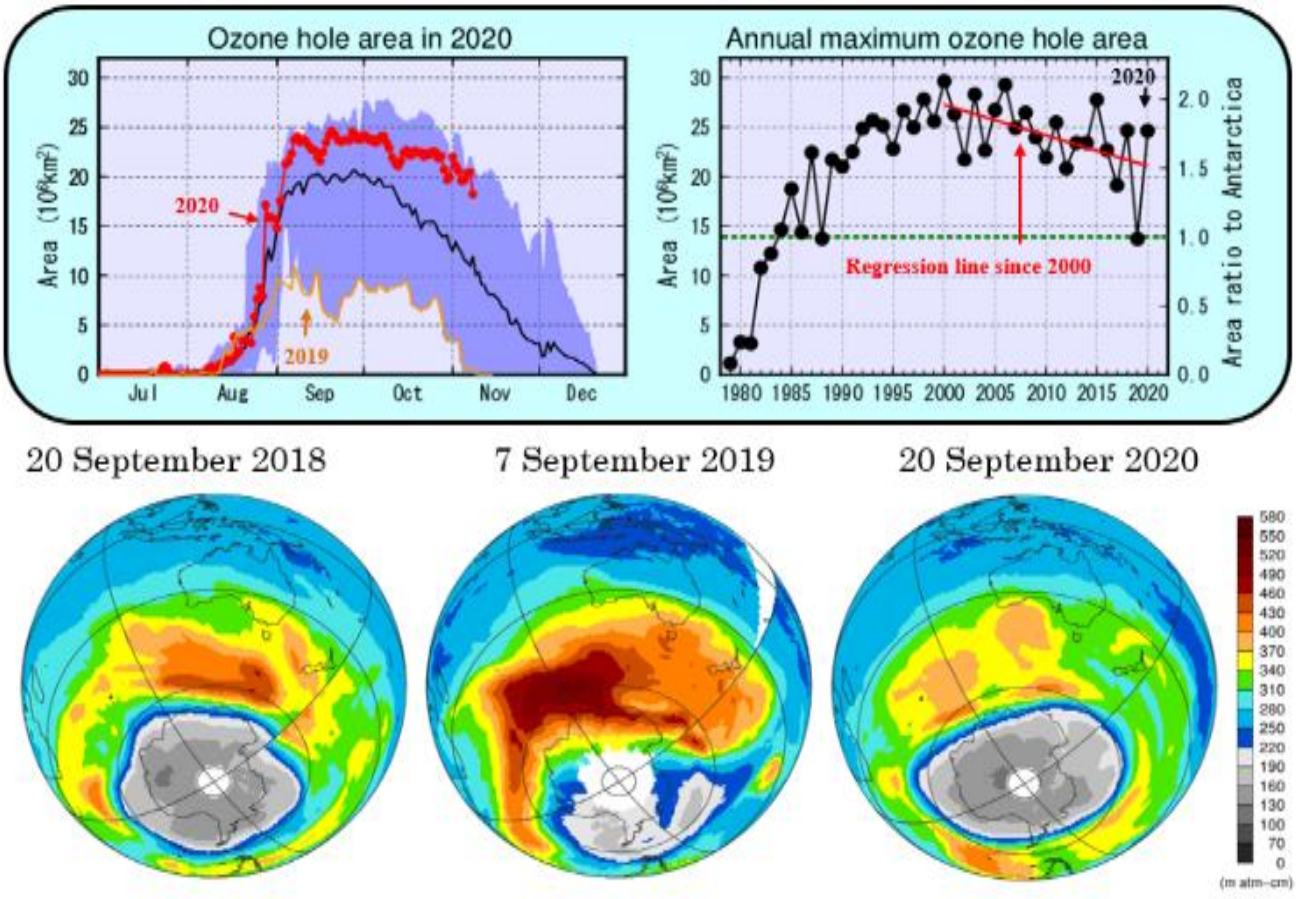

Figure 4-1 Antarctic ozone hole characteristics

Upper left: Time-series representation of the daily ozone hole area for 2020 (red line) and the 2010 – 2019 average (black line). Blue shading represents the range of daily maxima and minima over the previous 10 years.

Upper right: Inter-annual variability of the annual maximum ozone hole area. The green dotted line shows the area of the Antarctic Continent (13.9 million square kilometers).

Bottom: Snapshots of total column ozone distribution on the day of the annual maximum ozone hole area for the previous three years; the ozone hole is shown in grey (below 220 m atm-cm). Images are based on NASA satellite data.

Arctic sea ice extent in summer 2020

It is virtually certain that there has been a long-term decreasing trend of sea ice extent in the Arctic Ocean since 1979, when ongoing monitoring using similar satellite sensors began (statistically significant at a confidence level of 99%). The reduction in the annual minimum extent is particularly notable at 0.091 × 10^6 km^2 per year up to 2020 (Figure 5-1).

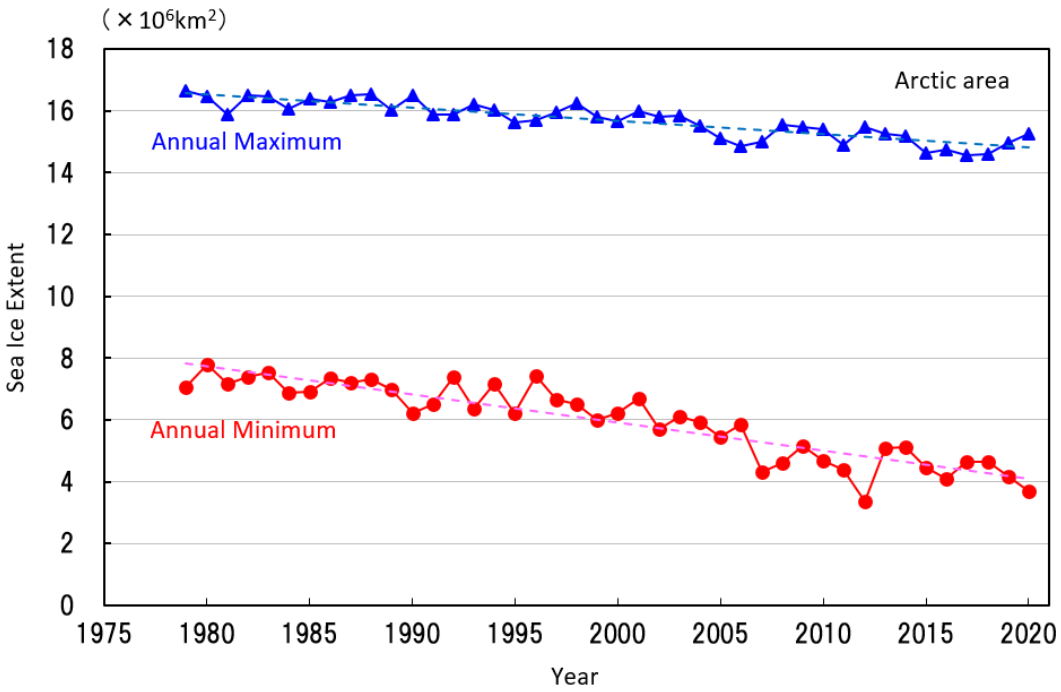

Figure 5-1 Time-series representations of annual maximum and annual minimum sea ice extent in the Arctic Ocean (including the Sea of Okhotsk and the Bering Sea) from 1979 to 2020

Blue and red lines indicate annual maximum means and annual minimum sea ice extents, respectively, with dashed lines indicating linear trends. Sea ice extents are calculated from brightness temperature data provided by NASA (the National Aeronautics and Space Administration) and NSIDC (the National Snow and Ice Data Center).

On March 3 2020, the preliminary annual maximum Arctic sea ice extent was 15.25 × 10^6 km^2, marking the 11th-lowest value since 1979. The value subsequently decreased during spring and summer in the Northern Hemisphere and reached its annual minimum of 3.69 × 10^6 km^2 on September 8, marking the second-lowest level since 1979 (Figures 5-2, 5-3).

(OKADA Ryohei, Office of Marine Prediction)

<<Table of contents <Top of this article

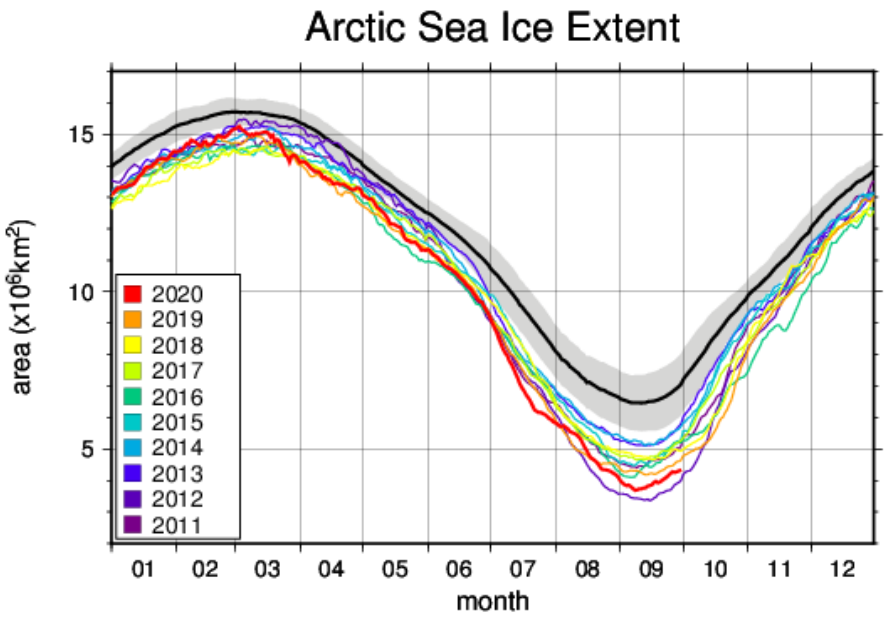

Figure 5-2 Annual variations in Arctic sea ice extent
The black line represents the normal, and shading represents the normal range.

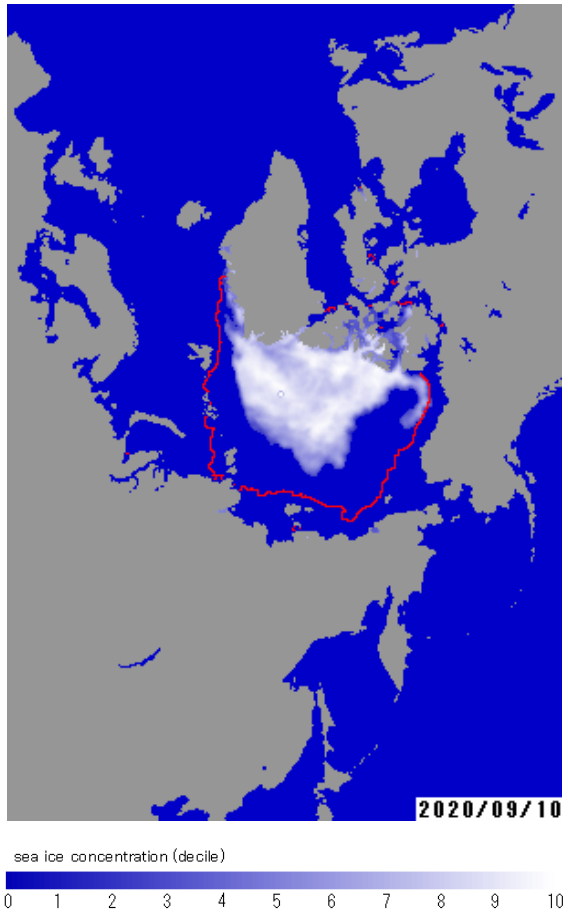

Figure 5-3 Annual minimum Arctic sea ice distribution
As of September 10 2020. The red line represents the normal extent.

The Eighth Session of the East Asia Winter Climate Outlook Forum (EASCOF-8)

The World Meteorological Organization (WMO) actively supports the activities of the Regional Climate Outlook Forums (RCOFs), which brings together experts from climatologically homogeneous regions and provides consensus-based seasonal predictions and information. As one of the RCOFs, the East Asia Winter Climate Outlook Forum (EASCOF) was jointly established by the China Meteorological Administration (CMA), the Japan Meteorological Agency (JMA), the Korea Meteorological Administration (KMA), and Mongolia's National Agency for Meteorology and Environment Monitoring (NAMEM) in 2012.

The eighth EASCOF session (EASCOF-8) was hosted online by JMA on 5 November 2020 with the presence of more than 30 experts from China, Japan, Mongolia and the Republic of Korea and a special contribution by experts from the North Eurasia Climate Centre (NEACC). Attendees discussed recent phenomena related to seasonal prediction of the East Asian Winter Monsoon (EAWM) and reached a consensus on seasonal outlooks for the coming winter. A WMO representative outlined the organization's objective seasonal prediction strategy, and a UN ESCAP representative detailed the organization's proposal for impact-based forecasting based on seasonal climate prediction in the region.

Even though the meeting was held online for the first time ever due to COVID-19, its discussions and expertise sharing helped to clarify understanding of climate dynamics related to EAWM and highlighted the importance of supporting climate service enhancement in individual countries.

Forum materials are available on the EASCOF portal at:
https://ds.data.jma.go.jp/tcc/tcc/library/EASCOF/index.html

(TSUJI Kazuaki, Tokyo Climate Center)

<<Table of contents <Top of this article

Figure 6-1 Attendees from KMA, JMA's Meteorological Research Institute, CMA, ESCAP, WMO's Regional Office for Asia and the South-West Pacific, NAMEM and JMA, with Tokyo Climate Center head FUJIKAWA Norihisa

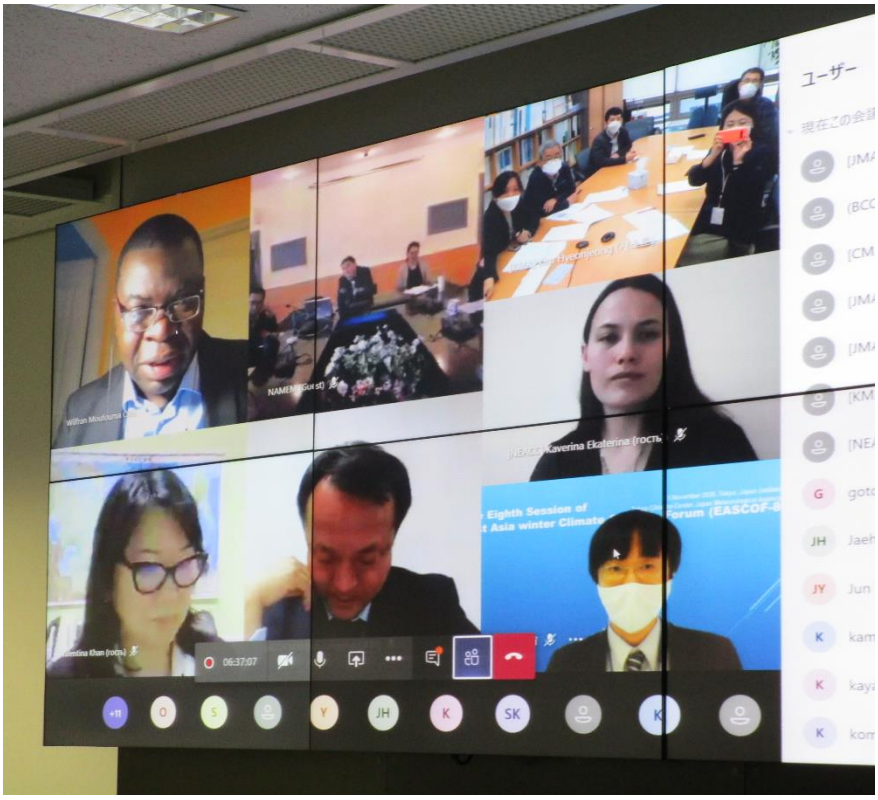

Figure 6-2 Attendees from WMO, NAMEM, KMA, NEACC, CMA, and JMA

JMA HQ relocation and reorganization

In autumn 2020, JMA relocated from its old HQ (built in 1964) to newly built premises around 3 km away, just south of Tokyo's Imperial Palace. The location is within walking distance of various major modern and historic tourist sites such as Zojoji Temple, Tokyo Tower and Toranomon Hills. The new premises are notable for their comprehensive state-of-the-art seismic insulation system, which is considered essential for such a facility in earthquake-prone Japan. TCC staff look forward to welcoming friends and colleagues from NMHSs worldwide to the offices.

JMA has also implemented one of its biggest-ever reorganizations to enhance its capacity for disaster response. Specifically, the new Atmosphere and Ocean Department now handles meteorological information including nowcasting, short/long-term forecasts and global climate change. Under this new structure, TCC remains committed to serving the climate community and performing its RCC duties.

Updated TCC/JMA address: 3-6-9 Toranomon, Minato City, Tokyo 105-8431, Japan

Email: tcc@met.kishou.go.jp (unchanged)

(Tokyo Climate Center)

<<Table of contents <Top of this article

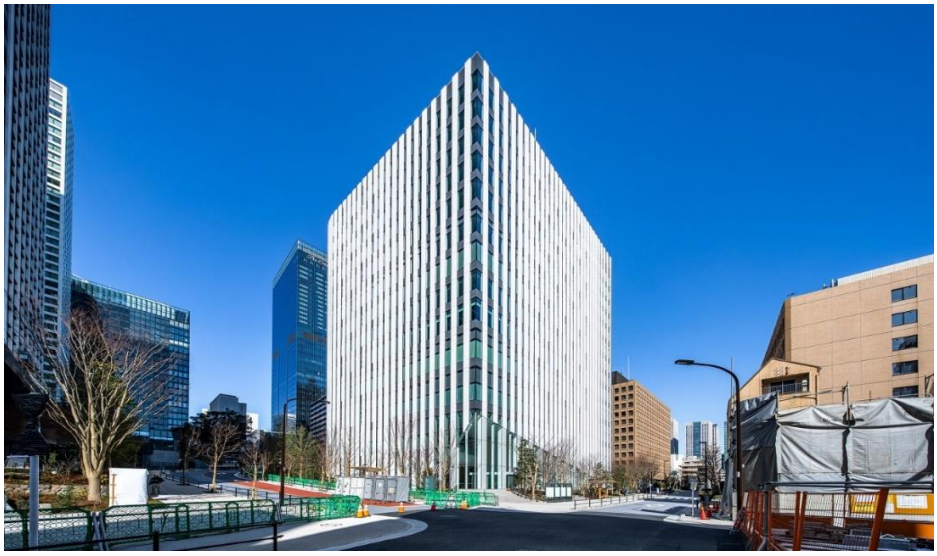

Figure 7-1 New JMA headquarter premises

You can also find the latest newsletter from Japan International Cooperation Agency (JICA).

JICA's World (October 2020)

https://www.jica.go.jp/english/publications/j-world/2010.html

JICA's World is the quarterly magazine published by JICA. It introduces various cooperation projects and partners along with the featured theme. The latest issue features "University Partnerships: Producing Future Leaders".

Any comments or inquiry on this newsletter and/or the TCC website would be much appreciated.
Please e-mail to tcc@met.kishou.go.jp.
(Editors: WAKAMATSU Shunya
and TSUJI Kazuaki)

Tokyo Climate Center, Japan Meteorological Agency

TCC Website:
https://ds.data.jma.go.jp/tcc/tcc/index.html